LETTERS

Detecting transient intermediates in macromolecular binding by paramagnetic NMR

Junji Iwahara[1] & G. Marius Clore[1]

Macromolecular complex formation is governed by two opposing constraints of specificity and speed[1,2]. Kinetic[3–6] and theoretical considerations suggest that significant rate enhancement can be achieved either by reducing the dimensionality of the search process[1,7] or by the creation of a short-range attractive potential around the target site[2]. This implies the existence of transient intermediates involving non-specific binding modes. Here we show that intermolecular paramagnetic relaxation enhancement (PRE) provides a means of directly detecting the presence of, and investigating the nature of, low population transient intermediates under equilibrium conditions. Applying this approach, we characterize the search process whereby a sequence-specific transcription factor (the homeodomain of HOXD9) binds to non-cognate DNA sites as a means of enhancing the rate of specific association. The PRE data in the fast exchange regime reveal the presence of transient intermediates formed in a stochastic manner at non-cognate sites whose structure is similar to that of the specific complex. Two distinct search processes involving intra- as well as intermolecular translocations can be delineated. The intermolecular PRE method is general and can be readily applied to investigations of transient intermediates in many other macromolecular binding processes.

The PRE is caused by magnetic dipolar interactions between a nucleus and the unpaired electrons of a paramagnetic centre, and results in an increase in the relaxation rate of the nuclear magnetization[8,9]. The magnitude of the PRE is proportional to $<r^{-6}>$ (where r is the distance between the nucleus of interest and the paramagnetic centre) and, owing to the large magnetic moment of an unpaired electron, the effect is detectable for sizeable separations (up to ~34 Å for Mn^{2+}). The impact on the transverse PRE, Γ_2, observed on the resonance of a major species A (99% occupancy) in a two-site exchange system comprising a minor species B (1% occupancy) with corresponding paramagnetic centre–proton distances of 30 Å and 8 Å, respectively, is shown in Fig. 1. (Γ_2 is defined as the difference in the transverse relaxation rates of the paramagnetic and diamagnetic states.) For a ~30-kilodalton (30-kDa) complex, the ^{1}H-Γ_2 arising from Mn^{2+} is ~2 s^{-1} ($\Gamma_{2,A}$) for species A but ~5.6×10^3 s^{-1} ($\Gamma_{2,B}$) for species B[10]. The apparent value of Γ_2 (Γ_2^{app}) is highly dependent on the exchange rate, k_{ex}, between the two species. If k_{ex} is slow (<50 s^{-1}), the presence of the minor species B has no effect and the value of Γ_2^{app} is the same as that expected for the major species A. For larger k_{ex}, however, Γ_2^{app} is highly influenced by the minor species B. When $k_{ex} \gg (\Gamma_{2,B}-\Gamma_{2,A})$, Γ_2^{app} is the weighted population average of the Γ_2 rates in the two species[11]. Under these conditions Γ_2^{app} is ~30-fold larger than $\Gamma_{2,A}$, thereby permitting one to both infer the presence of, and obtain some structural information on, a minor species.

We studied the interaction between the homeodomain of human HOXD9 and a 24-base-pair (24-bp) DNA duplex containing a single specific binding site (Fig. 2a). Conjugated deoxy (d)T-EDTA-Mn^{2+} (ref. 12; EDTA, ethylene diamine tetra-acetic acid) was placed at four distinct sites (one per duplex), two (sites 1 and 4) close to the ends of the DNA, and two (sites 2 and 3) adjacent to the 5′ and 3′ ends of the specific target site (Fig. 2a). Homeodomains are found in many eukaryotic transcription factors and possess well-characterized sequence-specific DNA-binding activity[13]. Because of the high degree of sequence identity to the *Drosophila* Antp homeodomain/DNA complex studied previously by both NMR[14] and crystallography[15], as well as the excellent agreement between measured dipolar couplings and those calculated from the related crystal structure[15] (dipolar coupling R-factor[16] of 14–15%, see Supplementary Information), the structure of the HOXD9 homeodomain/DNA complex can be readily

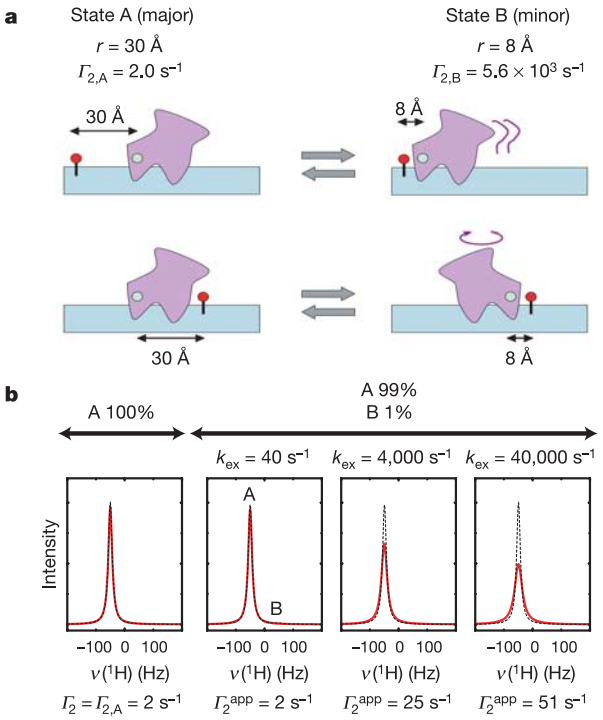

Figure 1 | Intermolecular PRE in an exchanging system. a, Exchange between two states A (major, 99%) and B (minor, 1%) in which the distance, r, from the monitored proton (green circle) on the protein (lilac) to the paramagnetic centre (red ball) on the DNA (cyan) is 30 Å and 8 Å, respectively. The transition between the two states may involve either translation (top) or rotation (bottom) of the protein relative to the DNA. **b**, Simulations based on the McConnell equation[27]. The solid red lines and dotted black lines represent NMR line-shapes with and without PRE, respectively (for details, see Supplementary Information). The definitions of Γ_2, Γ_2^{app}, $\Gamma_{2,A}$, $\Gamma_{2,B}$ and k_{ex} are given in the main text.

[1]Laboratory of Chemical Physics, National Institute of Diabetes and Digestive and Kidney Diseases, National Institutes of Health, Bethesda, Maryland 20892-0520, USA.

modelled. From two-dimensional ^{15}N-exchange spectroscopy, the apparent overall exchange rate for intermolecular translocation of the HOXD9 homeodomain between DNA specific sites (located on two DNA duplexes differing by only a single base pair just outside the specific binding site) is slow ($k_{ex} = 7\,s^{-1}$) on the NMR chemical shift timescale at 20 mM NaCl but fast ($k_{ex} \approx 600\,s^{-1}$) at 160 mM NaCl, under conditions where the concentration of total free DNA is ~200 μM (see Supplementary Information). The equilibrium dissociation constant (K_{diss}) measured by fluorescence anisotropy is 1.5 nM at 100 mM NaCl and 10 nM at 160 mM NaCl (Supplementary Information). ^1H_N-Γ_2 PREs were measured for the backbone amide groups (^1H_N) of complexed $^2H/^{15}N$-labelled HOXD9, and were found to be completely different in the slow- (Fig. 2b, 20 mM NaCl) and fast- (Fig. 2c, 100 and 160 mM NaCl) exchange regimes for all four dT-EDTA-Mn^{2+} sites (see Supplementary Information).

Under the experimental conditions employed, involving relatively high (submillimolar) concentrations of free DNA, the exchange process observed in the ^{15}N-exchange experiments does not involve spontaneous dissociation of the protein followed by reassociation of free protein and DNA, but occurs via direct transfer following collision of free DNA with DNA-bound protein to form a transient ternary encounter complex without ever going through the intermediary of free protein[17]. This mechanism, which is akin to intersegment transfer[3], dramatically accelerates the rate of target recognition in protein–DNA interactions, resulting in translocation rates that are over 3 orders of magnitude faster than the dissociation rate constant determined by gel shift assays at very low (nM) concentrations of free DNA ($k_{diss} \ll 0.01\,s^{-1}$ for the HOXD9 homeodomain)[18,19]. This reconciles the highly dynamic behaviour of protein–DNA complexes observed *in vivo* using microscopy combined with photobleaching techniques[20] with the long half-lives of specific protein–DNA complexes measured by traditional biochemical analysis *in vitro*[17].

At 20 mM NaCl, the ^1H_N-Γ_2 data arising from the four dT-EDTA-Mn^{2+} groups are fully consistent with the structure of the complex bound to the specific site (Figs 2b and 3c; see also Supplementary Information). Large magnitude ^1H_N-Γ_2 PREs ($>10\,s^{-1}$) are only observed for those regions in relatively close proximity to the dT-EDTA-Mn^{2+} groups, and the observed ^1H_N-Γ_2 values are in excellent agreement with those predicted from the model of the specific complex with an overall PRE *Q*-factor[10] of 0.26 (Fig. 2d). Thus, in the slow exchange regime, the presence of intermediate states, as expected from the lineshape simulations shown in Fig. 1, is not apparent from the PRE data.

At 100 and 160 mM NaCl, however, many residues exhibit ^1H_N-Γ_2 PREs that are completely inconsistent with the structure of the specific complex (Figs 2c, e and 3d, and Supplementary Fig. S3).

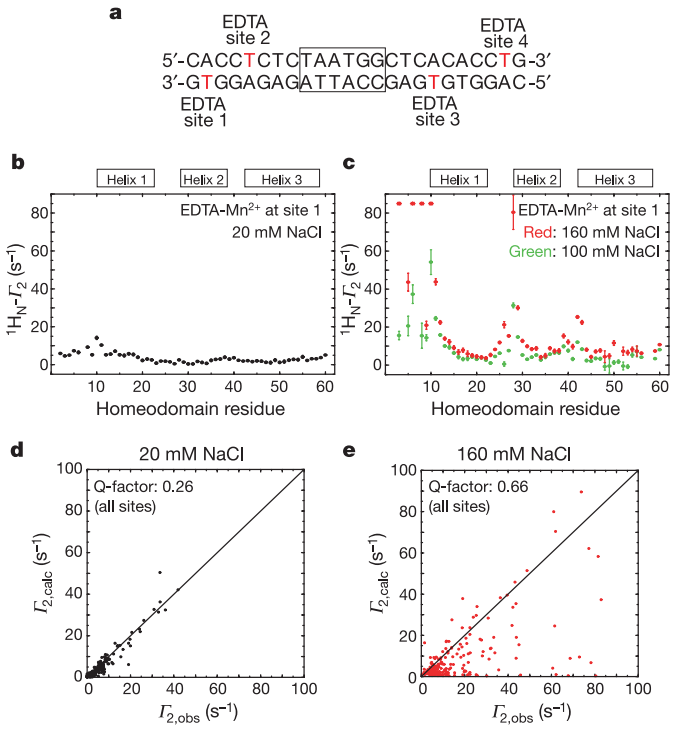

Figure 2 | Intermolecular PRE for the HOXD9 homeodomain/DNA complex in slow and fast exchange. **a**, 24-bp duplex DNA. The specific target site (TAATGG) is boxed. The four sites chosen to covalently attach EDTA to thymine (one site at a time) are shown in red. **b**, **c**, Intermolecular PRE ^1H_N-Γ_2 profiles obtained for EDTA-Mn^{2+} at site 1 in 20 mM (**b**), 100 mM (**c**, green) and 160 mM (**c**, red) NaCl. Asterisks indicate residues whose $^1H_N/^{15}N$ cross-peaks are broadened beyond the limits of detection. Γ_2 profiles for sites 2–4 are shown in Supplementary Fig. S3. **d**, **e**, Correlation between observed and calculated PREs at all 4 sites in 20 mM (**d**) and 160 mM (**e**) NaCl (217 and 197 data points, respectively). The PRE Q-factor[10] is a measure of agreement between observed and calculated values of Γ_2 and is given by $[\sum_i\{\Gamma_2^{obs}(i) - \Gamma_2^{calc}(i)\}^2 / \sum_i \Gamma_2^{obs}(i)^2]^{1/2}$. Error bars, ±1 s.d.

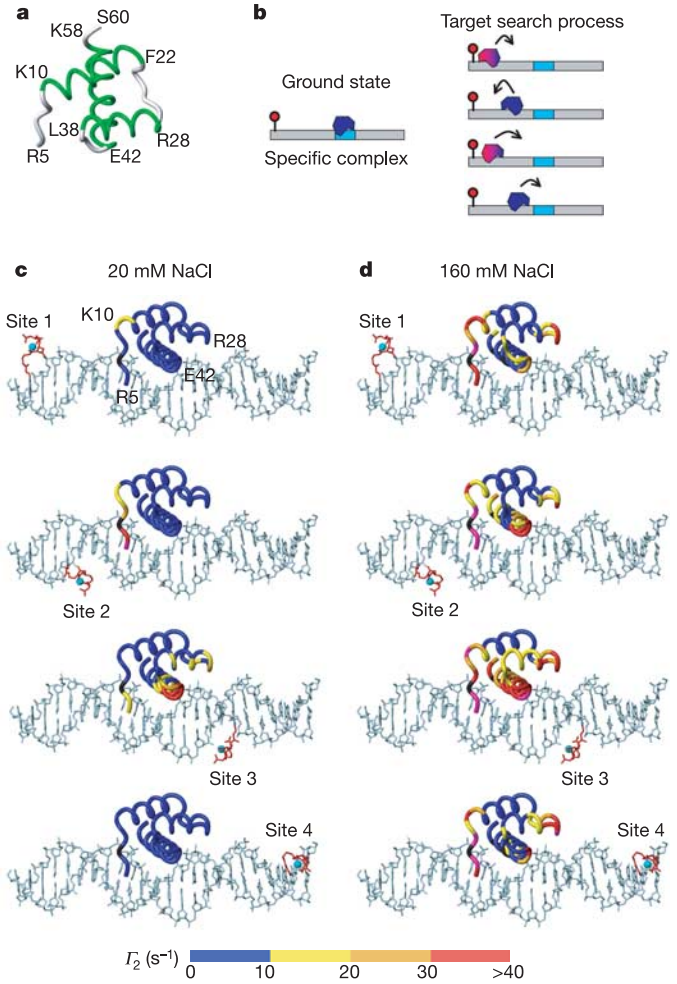

Figure 3 | Summary of the intermolecular PRE profiles arising from dT-EDTA-Mn^{2+} at sites 1 to 4 for the HOXD9 homeodomain/DNA complex in the slow and fast exchange regimes. **a**, Ribbon diagram of the HOXD9 homeodomain. **b**, Schematic representation of the specific target search process involving non-specific binding intermediates that experience strong intermolecular PRE (indicated by the colour gradient from red to blue, with red indicating strong PRE). **c**, **d**, Intermolecular PRE ^1H_N-Γ_2 data from sites 1 to 4 at 20 mM (**c**) and 160 mM (**d**) NaCl mapped on the structural model of the HOXD9/DNA complex: colour scale shows Γ_2.

For example, Arg 28 and Asp 29 (at the amino terminus of helix 2) exhibit $^{1}H_N$-Γ_2 values $>30\,s^{-1}$ but in the specific complex are located on the opposite face of the protein with respect to dT-EDTA-Mn^{2+} at sites 1 and 2 with corresponding Mn^{2+}–$^{1}H_N$ distances >40 Å. The carboxy-terminal half of helix 1 (Glu 15 to Asn 23) is closer to dT-EDTA-Mn^{2+} at sites 1 and 2 than Arg 28 and Asp 29, yet displays $^{1}H_N$-Γ_2 values $<10\,s^{-1}$ that are minimally affected by salt concentration. The dramatic changes in $^{1}H_N$-Γ_2 PRE profiles upon increasing the ionic strength from 20 to 160 mM NaCl are not due to any significant structural changes in the specific complex, because (1) the ^{1}H–^{15}N correlation spectrum of the HOXD9 homeodomain bound to DNA is essentially identical at 20 and 160 mM NaCl, and (2) the residual dipolar couplings at the two salt conditions are highly correlated (correlation coefficient, 0.99; see Supplementary Fig. S2). We therefore conclude that the intermolecular PRE data at 100 and 160 mM NaCl represent the footprint of minor species that exchange rapidly with the specific complex. The HOXD9 homeodomain in these minor states is bound in a stochastic manner to various sites on the DNA, and can be located in close spatial proximity to the dT-EDTA-Mn^{2+} sites. The population of the minor species is less than 1%, judging from the values of the specific and non-specific equilibrium dissociation constants (1.5 versus 270 nM at 100 mM NaCl).

The overall PRE profiles at 160 mM NaCl also provide structural information relating to non-specific DNA binding of the HOXD9 homeodomain. Patches on the protein with large PREs (Fig. 3d) indicate that these regions can come into close proximity to conjugated dT-EDTA-Mn^{2+} located in the DNA major groove, while regions with small PREs, such as the C-terminal half of helix 1 (Glu 15–Asn 23), must be distant from the DNA interface even in the non-specific complexes. The PRE map therefore suggests that the DNA binding mode adopted during the target search process is similar to that in the specific complex, and that the populations of any potential species involving alternative protein interaction surfaces, should these exist, are below the limits of detection.

The target search process can involve either intramolecular translocation of the protein (for example, sliding or one-dimensional diffusion along the DNA) or intermolecular translocation in which the protein is directly transferred from one DNA molecule to another (Fig. 4a). To evaluate their relative contributions, we carried out additional PRE experiments on two samples comprising an equal mixture of two DNA duplexes, one with and the other without the specific target site. EDTA-Mn^{2+} was conjugated to the non-specific DNA duplex in sample 1 and to the specific DNA duplex in sample 2 (Fig. 4b). Thus, for sample 1 the intermolecular PRE can only arise through intermolecular translocation, while for sample 2 both intra- and intermolecular processes can contribute. The ^{1}H–^{15}N correlation spectrum of HOXD9 in both samples was basically the same as that of the specific complex, indicating that essentially all protein is bound to the specific target site (see Supplementary Fig. S4). The PRE profiles observed for the two samples at 160 mM NaCl (Fig. 4c) are similar, but the magnitude of the PREs for sample 2 are generally larger than those for sample 1, indicating that both intra- and intermolecular translocations are involved in the target search. From the ratio of the Γ_2 values for samples 1 and 2 (Fig. 4c), the contribution of intermolecular translocation is actually larger than that of intramolecular translocation. This is due to the high total concentration of free DNA (0.8 mM) in the NMR samples. As the concentration of DNA in the nucleus is as high as $\sim 100\,mg\,ml^{-1}$ (equivalent to 150 mM on a per base pair basis)[21], it seems quite feasible that intermolecular translocation (or intersegment transfer) could contribute significantly to the speed of the search process *in vivo*[17]. Quantitative analysis of the PRE data for samples 1 and 2 also reveals the existence of one-dimensional sliding along the DNA. For Met 24–Glu 33 and Thr 41–Glu 42, the PREs measured for sample 2 are systematically larger by ~30–100% than those for sample 1, whereas those for the N-terminal arm region are almost the same for samples 1 and 2 (Fig. 4c). These observations can be attributed to bias in which the orientation of the protein bound to the specific site is favoured as the protein slides (intra-molecular translocation) along DNA. Thus, in the sliding process the segments Met 24–Glu 33 and Thr 41–Glu 42 can come very close to the EDTA-Mn^{2+} on the oligonucleotide containing the specific target site in sample 2 (DNA 2A in Fig. 4b) whereas the N-terminal arm cannot be so close unless the protein takes up the opposite orientation on the DNA, which is allowed by intermolecular translocation (see Fig. 4d).

In conclusion, intermolecular PRE data for complexes in the fast exchange regime can provide valuable information on intermediates

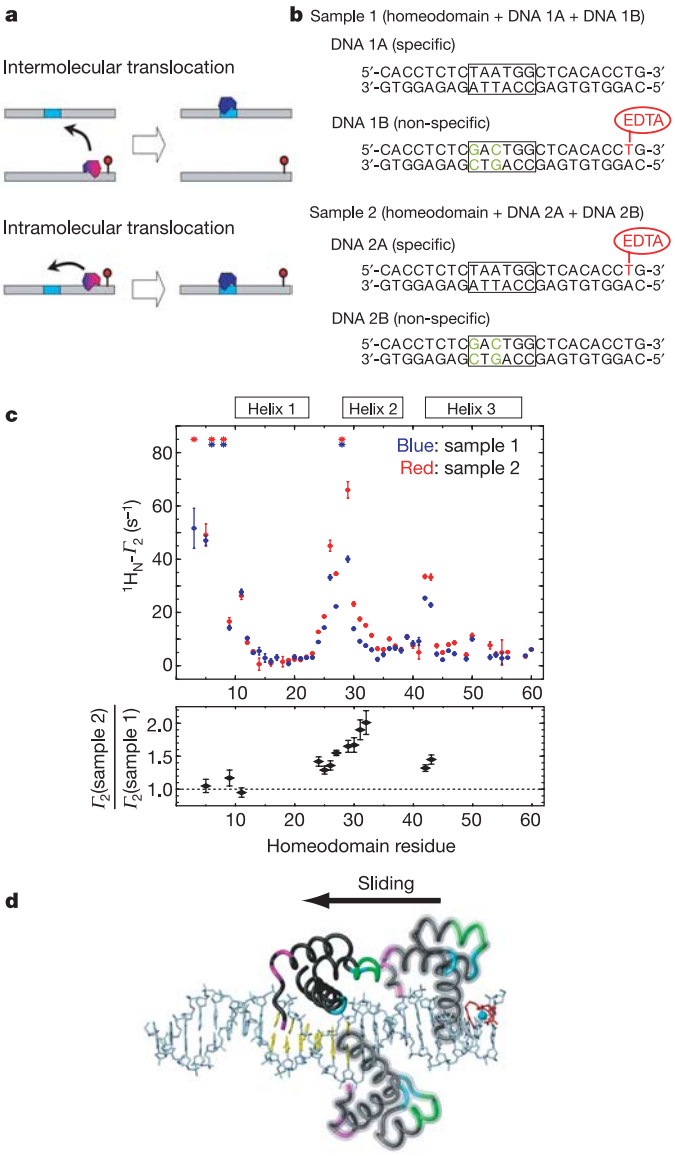

Figure 4 | Intermolecular PRE arises from inter- and intramolecular translocation processes. **a**, Diagrammatic representation of inter- and intramolecular translocation giving rise to observable PREs. **b**, DNA samples. **c**, PRE data for samples 1 (blue) and 2 (red) are displayed on the top panel (asterisks represent cross-peaks broadened beyond the limits of detection); the bottom panel shows the Γ_2(sample 2)/Γ_2(sample 1) ratios for residues with $\Gamma_2 > 12\,s^{-1}$ in sample 2. **d**, Schematic representation of sliding along the DNA: homeodomain residues with Γ_2(sample 2)/Γ_2(sample 1) ratio <1.25, magenta; 1.25 to 1.5, cyan; and >1.5, green. The specific DNA target site is coloured in yellow. Specifically and non-specifically (two) bound homeodomains are depicted as opaque and transparent tubes, respectively. Error bars, ±1 s.d.

whose populations at equilibrium are very low. These measurements not only reveal the presence of intermediate states but also shed light on their structural features. Although the methodology was applied to a protein–DNA complex, a similar approach can be equally well applied to protein–protein complexes (unpublished data), as extrinsic paramagnetic groups can be readily linked covalently to proteins via surface cysteine residues (selectively introduced by mutagenesis)[22,23]. Experimental data on the detection of low populations of intermediates at equilibrium, together with appropriate computational studies, such as brownian dynamics simulations[24], should yield a deeper insight into macromolecular recognition processes.

METHODS

Sample preparation. The human HOXD9 homeodomain was prepared as described[17]. 24-bp DNA fragments with and without dT-EDTA were prepared as described[10–12]. To make metal-free samples of DNA, free EDTA (50 mM) was initially added and then removed by exchanging the buffer to 20 mM Tris HCl (pH 6.8), 500 mM NaCl, using an Amicon Ultra spin concentrator. The EDTA-conjugated DNA in the apo-state was mixed with metal ions (Mn^{2+} or Ca^{2+}) in ~50% excess relative to DNA. The HOXD9 homeodomain was added to the mixture at a protein-to-DNA ratio of 1:1.5 in the presence of 500 mM NaCl. The excess metal ions located at sites other than the conjugated EDTA were removed by extensive washing with 20 mM Tris HCl (pH 6.8) and 500 mM NaCl using a spin concentrator. After washing, the buffer for the HOXD9/DNA-EDTA-metal complexes was exchanged to 10 mM Tris HCl (pH 6.8), 20 mM NaCl and 7% D_2O for NMR measurements. All buffers were treated with chelex-20 (Sigma) to avoid contamination of metal ions.

NMR spectroscopy. ^1H-, ^{13}C- and ^{15}N-resonances were assigned as described[17]. PRE ^1H_N-Γ_2 data at a ^1H frequency of 600 MHz were acquired at 35 °C using Bruker DRX-600 spectrometers equipped with cryogenic triple resonance probes. For individual PRE experiments, data on two samples comprising 0.4 mM $^2H/^{15}N$-labelled HOXD9 homeodomain and 0.6 mM DNA-EDTA chelating either Ca^{2+} or Mn^{2+} were recorded, using two-dimensional ^1H–^{15}N correlation spectra described previously[12,25]. The protein NMR chemical shifts for the Mn^{2+} and Ca^{2+} chelated states are identical as the *g*-tensor for Mn^{2+} is isotropic. Two time points with a difference of 14 ms were used for PRE ^1H_N-Γ_2 measurements. Values of ^1H_N-Γ_2 were calculated as described[10]. For the complex comprising dT-EDTA at site 4, the ^1H-relaxation rates were also measured with eight ^1H relaxation time points and the values of ^1H_N-Γ_2 obtained were identical to those from the data recorded at two time points within experimental errors. The maximum value of Γ_2 that can be determined accurately is ~80–90 s^{-1}; beyond that, the ^1H_N–^{15}N cross-peaks are too broad to permit quantitative determination of the PRE.

Two samples were employed to analyse the contribution of intra- and intermolecular translocation processes to the intermolecular PRE (Fig. 4b). Sample 1 comprised $^2H/^{15}N$-labelled HOXD9 homeodomain, DNA 1A (containing the specific target site but no EDTA-conjugation), and DNA 1B (with EDTA-conjugation at a position corresponding to site 4 and the specific target site removed by two base pair mutations). Sample 2 contained $^2H/^{15}N$-labelled HOXD9 homeodomain, DNA 2A (containing the specific DNA target site and EDTA-Mn^{2+} conjugation at site 4) and DNA 2B (without specific target site and no EDTA-Mn^{2+} conjugation). The only difference between samples 1 and 2 is the location of the conjugated EDTA-Mn^{2+} (that is, on the DNA containing the specific target site in sample 2 and on the DNA with the specific target site removed in sample 1). The ratio of protein:$DNA_{specific}$:$DNA_{non\text{-}specific}$ was 1:1.5:1.5 with a protein concentration of 0.4 mM.

Back-calculation of PREs. PREs were back-calculated from the structural model of the HOXD9/DNA complex using a three-conformer ensemble representation for the EDTA-Mn^{2+} groups to account for their flexibility[10]. The coordinates of the EDTA-Mn^{2+} moieties were optimized by simulated annealing using Xplor-NIH[26] as described previously[10].

Received 28 November 2005; accepted 22 February 2006.

1. Berg, O. G. & von Hippel, P. H. Diffusion-controlled macromolecular interactions. *Annu. Rev. Biophys. Biophys. Chem.* **14,** 131–160 (1985).
2. Zhou, H.-X. & Szabo, A. Enhancement of association rates by nonspecific binding to DNA and cell membranes. *Phys. Rev. Lett.* **93,** 178101 (2004).
3. von Hippel, P. H. & Berg, O. G. Facilitated target location in biological systems. *J. Biol. Chem.* **264,** 675–678 (1989).
4. Halford, S. E. & Marko, J. F. How do site-specific DNA-binding proteins find their targets? *Nucleic Acids Res.* **32,** 3040–3052 (2004).
5. Schreiber, G. & Fersht, A. R. Rapid, electrostatically assisted association of proteins. *Nature Struct. Biol.* **3,** 427–431 (1996).
6. Vijayakumar, M. *et al.* Electrostatic enhancement of diffusion-controlled protein-protein association: comparison of theory and experiment on barnase and barstar. *J. Mol. Biol.* **278,** 1015–1024 (1998).
7. Adam, G. & Delbruck, M. in *Structural Chemistry and Molecular Biology* (eds Rich, A. & Davidson, N.) 198–215 (Freeman & Co., San Francisco, 1968).
8. Solomon, I. Relaxation processes in a system of two spins. *Phys. Rev.* **99,** 559–565 (1955).
9. Bloembergen, N. & Morgan, L. O. Proton relaxation times in paramagnetic solutions. Effects of election spin relaxation. *J. Chem. Phys.* **34,** 842–850 (1961).
10. Iwahara, J., Schwieters, C. D. & Clore, G. M. Ensemble approach for NMR structure refinement against ^1H paramagnetic relaxation enhancement data arising from a flexible paramagnetic group attached to a macromolecule. *J. Am. Chem. Soc.* **126,** 5879–5896 (2004).
11. Iwahara, J., Schwieters, C. D. & Clore, G. M. Characterization of nonspecific protein-DNA interactions by ^1H paramagnetic relaxation enhancement. *J. Am. Chem. Soc.* **126,** 12800–12808 (2004).
12. Iwahara, J., Anderson, D. E., Murphy, E. C. & Clore, G. M. EDTA-derivatized deoxythymidine as a tool for rapid determination of protein binding polarity to DNA by intermolecular paramagnetic relaxation enhancement. *J. Am. Chem. Soc.* **125,** 6634–6635 (2003).
13. Gehring, W. J. *et al.* Homeodomain-DNA recognition. *Cell* **78,** 211–223 (1994).
14. Billeter, M. *et al.* Determination of the nuclear magnetic resonance solution structure of an Antennapedia homeodomain-DNA complex. *J. Mol. Biol.* **234,** 1084–1093 (1993).
15. Fraenkel, E. & Pabo, C. O. Comparison of X-ray and NMR structures for the Antennapedia homeodomain-DNA complex. *Nature Struct. Biol.* **5,** 692–697 (1998).
16. Clore, G. M. & Garrett, D. S. R-factor, free R and complete cross-validation for dipolar coupling refinement of NMR structures. *J. Am. Chem. Soc.* **121,** 9008–9012 (1999).
17. Iwahara, J. & Clore, G. M. Direct observation of enhanced translocation of a homeodomain between DNA cognate sites by NMR exchange spectroscopy. *J. Am. Chem. Soc.* **128,** 404–405 (2006).
18. Affolter, M., Percival-Smith, A., Müller, M., Leupin, W. & Gehring, W. J. DNA binding properties of the purified Antennapedia homeodomain. *Proc. Natl Acad. Sci. USA* **87,** 4093–4097 (1990).
19. Catron, K. M., Iler, N. & Abate, C. Nucleotides flanking a conserved TAAT core dictate the DNA binding specificity of three murine homeodomain proteins. *Mol. Cell. Biol.* **13,** 2354–2365 (1993).
20. Misteli, T. Protein dynamics: implications for nuclear architecture and gene expression. *Science* **291,** 843–847 (2001).
21. Lewin, B. *Genes VII* (Oxford Univ. Press, Oxford, 2000).
22. Gillespie, J. R. & Shortle, D. Characterization of long-range structure in the denatured state of staphylococcal nuclease. I. Paramagnetic relaxation enhancement by nitroxide spin labels. *J. Mol. Biol.* **268,** 158–169 (1997).
23. Dvoretsky, A., Gaponenko, V. & Rosevear, P. R. Derivation of structural restraints using a thiol-reactive chelator. *FEBS Lett.* **528,** 189–192 (2002).
24. Gabdoulline, R. R. & Wade, R. C. Biomolecular diffusional association. *Curr. Opin. Struct. Biol.* **12,** 204–213 (2002).
25. Donaldson, L. W. *et al.* Structural characterization of proteins with an attached ATCUN motif by paramagnetic relaxation enhancement NMR spectroscopy. *J. Am. Chem. Soc.* **123,** 9843–9847 (2001).
26. Schwieters, C. D., Kuszewski, J., Tjandra, N. & Clore, G. M. The Xplor-NIH NMR molecular structure determination package. *J. Magn. Reson.* **160,** 65–73 (2003).
27. McConnell, H. M. Reaction rates by nuclear magnetic resonance. *J. Chem. Phys.* **28,** 430–431 (1958).

Supplementary Information is linked to the online version of the paper at www.nature.com/nature.

Acknowledgements This work was supported by the Intramural Program of the NIH, the NIDDK, and in part by the AIDS Targeted Antiviral Program of the Office of the Director of the NIH (G.M.C.).

Author Information Reprints and permissions information is available at npg.nature.com/reprintsandpermissions. The authors declare no competing financial interests. Correspondence and requests for materials should be addressed to G.M.C. (mariusc@intra.niddk.nih.gov).